

Bimetallic Gold(I) Complexes with Ethynyl-Helicene and Bis-Phosphole Ligands: Understanding the Role of Aurophilic Interactions in their Chiroptical Properties

Mehdi El sayed moussa, Hui Chen, Zuoyong Wang, Monika Srebro-Hooper, Nicolas Vanthuyne, Soizic Chevance, Christian Roussel, J. A. Gareth Williams, Jochen Autschbach, Régis Réau, et al.

▶ **To cite this version:**

Mehdi El sayed moussa, Hui Chen, Zuoyong Wang, Monika Srebro-Hooper, Nicolas Vanthuyne, et al.. Bimetallic Gold(I) Complexes with Ethynyl-Helicene and Bis-Phosphole Ligands: Understanding the Role of Aurophilic Interactions in their Chiroptical Properties. Chemistry - A European Journal, 2016, 22 (17), pp.6075-6086. 10.1002/chem.201600126 . hal-01292929

HAL Id: hal-01292929

https://univ-rennes.hal.science/hal-01292929

Submitted on 2 Jun 2016

HAL is a multi-disciplinary open access archive for the deposit and dissemination of scientific research documents, whether they are published or not. The documents may come from teaching and research institutions in France or abroad, or from public or private research centers.

L'archive ouverte pluridisciplinaire **HAL**, est destinée au dépôt et à la diffusion de documents scientifiques de niveau recherche, publiés ou non, émanant des établissements d'enseignement et de recherche français ou étrangers, des laboratoires publics ou privés.

Bimetallic gold(I) complexes with ethynyl-helicene and bis-phosphole ligands: understanding the role of aurophillic interaction in their chiroptical properties

Mehdi El Sayed Moussa,[a] Hui Chen,[b,c] Zuoyong Wang,[b] Monika Srebro-Hooper,[d] Nicolas Vanthuyne,[e] Soizic Chevance,[a] Christian Roussel,[e] J. A. Gareth Williams,[f] Jochen Autschbach,*[,g] Régis Réau,[a] Zheng Duan,*[,b] Christophe Lescop,*[,a] and Jeanne Crassous*[,a]

Abstract: Monometallic gold(I)-alkynyl-helicene complexes (**1a**,**b**,) and bimetallic gold(I)-alkynyl-helicene architectures featuring the presence (**2a**,**b**) or absence (**3a**,**b**) of aurophillic intramolecular interactions were prepared by using different types of phosphole ligands (mono-phosphole **L1** or bis-phospholes **L2**,**3**). The influence of the Au(I) d^{10}-metal center(s) on the electronic, photophysical and chiroptical properties of these unprecedented phosphole-gold(I)-alkynyl-helicene complexes were examined. Experimental and theoretical results highlight the importance of ligand-to-ligand-type charge transfers and the strong effect of presence or absence of Au(I)-Au(I) interactions in **2a**,**b**.

Introduction

Among the non-covalent interactions available in the toolbox of supramolecular chemistry, metal-metal interactions between d^{10} closed-shell metal ions have been used to complement H-bonding, van der Waals interactions or π-π interactions in order to direct the relative conformation of isolated molecules and to drive self-assembling processes leading to the formation of complex superstructures.[1] The Au(I)-Au(I) metallophillic interaction is particularly strong. Ranging within about 7-12 kcal/mol, its strength is comparable to that of a hydrogen bond.[2] In addition, the rich emission properties that often arise from these d^{10}-d^{10} closed-shell metal-metal interactions can be preserved in the resulting supramolecular structure, paving the way to functional supramolecular material bearing original optoelectronic properties.[3] Although aurophillic interactions have attracted increasing interest in crystal engineering and material sciences, they have been used only scarcely as structuring agents in the design of enantiopure supramolecular assemblies and the modulation of their chiroptical properties.[4] This is rather surprising, because considerable effort has been devoted in the last decade to the construction of chiral metal-based supramolecular assemblies for their potential applications as helical polymers,[5a] liquid crystals,[5b] chiral metal-organic frameworks (MOFs),[5c] chiral cages,[5d] asymmetric catalysts,[5e] or as advanced functional materials.[5f-h]

Among the chiral fragments used in molecular engineering, helicene moieties are promising chiral π-conjugated building blocks for new functional molecular materials since they bear large-magnitude chiroptical properties related to their helical backbones, such as high optical rotation values, strong circular dichroism, and sometimes intense circularly polarized luminescence.[6] Therefore they may be used to construct novel chiral architectures with targeted applications such as in fibers and gels, liquid crystals, switches, circularly polarized absorbers and emitters, to name just a few.[6,7] Interestingly, the coordination and organometallic chemistry of helicene-based ligands have recently highlighted the key role played by the metal center in order to direct the spatial organization of the helicene fragments and/or to induce unique photophysical and chiroptical properties within the resulting derivatives.[6i]

On the other hand, extended π-conjugated molecules based on phospholes decorated with aromatics, and their transition-metal complexes, have been shown to display a wide range of electronic and optical properties for applications in optoelectronics.[8] For instance, some of us have shown that the molecular engineering of 2,2'-bisphosphole units by metal coordination can lead to strongly emissive molecular architectures with applications as dopants in organic light emitting diodes (OLEDs).[9] These observations prompted us to study how the structuring agent/property carrier duality of the aurophillic interactions could lead to chiral systems based on bimetallic gold complexes bearing helicene substituents with controlled topology (Figure 1), and to rationalize its impact on the electronic, photophysical and chiroptical properties. Specifically, considering that gold(I)-alkynyl complexes have attracted particular attention due to their many potential applications as luminescent molecular materials[3e-h], and that among all these derivatives, the gold(I)-

[a] Institut des Sciences Chimiques de Rennes, UMR 6226, Campus de Beaulieu, CNRS-Université de Rennes 1, 35042 Rennes Cedex, France. E-mail: christophe.lecop@univ-rennes1.fr, jeanne.crassous@univ-rennes1.fr.
[b] College of Chemistry and Molecular Engineering, International Phosphorus Laboratory, International Joint Research Laboratory for Functional Organophosphorus Materials of Henan Province, Zhengzhou University, Zhengzhou 450001, P. R. China. E-mail: duanzheng@zzu.edu.cn.
[c] Institute of Chemistry Henan Academy of Sciences, Zhengzhou 450002 , P. R. China.
[d] Faculty of Chemistry, Jagiellonian University, 30-060 Krakow, Poland.
[e] Aix Marseille Université, Centrale Marseille, CNRS, iSm2 UMR 7313, 13397, Marseille, France.
[f] Department of Chemistry, University of Durham, Durham, DH1 3LE, UK,
[g] Department of Chemistry, University at Buffalo, State University of New York, Buffalo, NY 14260, USA. E-mail: jochena@buffalo.edu.

Supplementary information for this article is given via a link at the end of the document.

ethynyl compounds stabilized by an auxiliary phosphane ligand represent a major class of luminescent complexes[3e-h,10], we have focused our interest on stable gold(I) organometallic architectures pre-assembled by phosphole and bis-phosphole ligands and grafted by alkynyl-helicenes (Figure 1).[11]

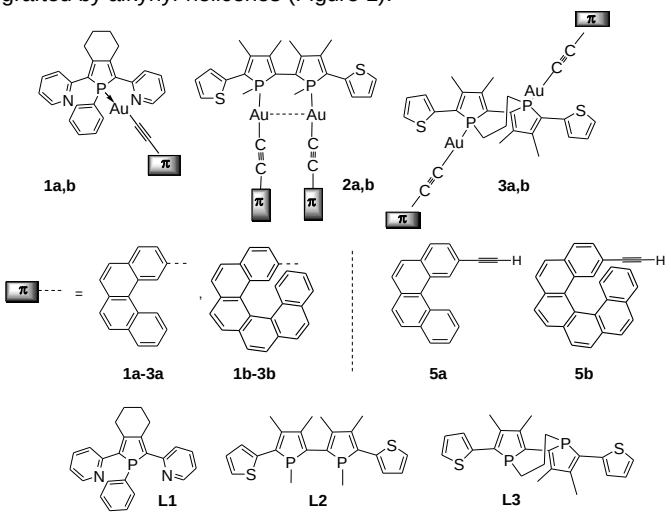


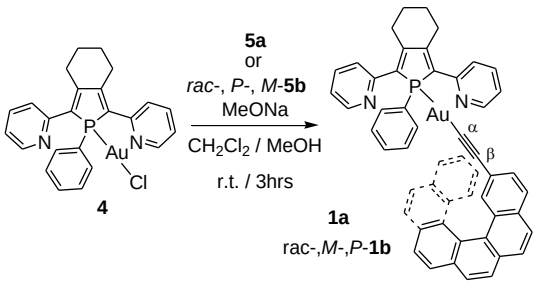
Figure 1. Mono-gold (**1a**,**b**) and bis-gold complexes (**2a**,**b** and **3a**,**b**) either promoting gold-gold interaction or not and respectively bearing phosphole ligands **L1**, **L2** or **L3** and ethynyl-helicene ligands **5a** or **5b**.

Herein, we describe the synthesis, structural and spectroscopic characterization of six unprecedented phosphople-Au(I)-alkynyl complexes bearing helicene π-units on the alkynyl fragment, including their enantiopure derivatives. Their electronic, photophysical and unique chiroptical properties are reported along with corresponding first-principles calculations (at the Kohn-Sham (KS) and time-dependent KS (TDKS) level) aimed at highlighting the fascinating electronic structures of this new series of chiral Au(I) complexes. In the first stage, the synthesis of monometallic Au(I) complexes (**1a**,**b** in Figure 1) stabilized by a monophosphole ligand (**L1**) and grafted by one 2-ethynyl-[4]helicene (**5a**) or one 2-ethynyl-[6]helicene (**5b**) ligand have been performed and their properties have been examined, in order to evaluate how the formation of the Au(I)-alkynyl bond impacts the electronic structure of the helicene fragment and its chiroptical activity. In the second stage, the coordination of two **5a** or **5b** ligands onto two different bimetallic Au(I) precursors has been carried out, yielding distinct structural types of bimetallic architecture (**2a**,**b** and **3a**,**b** in Figure 1). (*i*) The use of a U-shaped bimetallic Au(I) precursor bearing a 2,2'-bisphosphole unit (**L2**) led to scaffolds **2a**,**b** that are stabilized by a Au(I)-Au(I) intramolecular interaction. (*ii*) Meanwhile, a Z-shaped bimetallic Au(I) precursor based on a 2,2'-bisphosphole unit (**L3**), whose intrinsic structure prevents aurophillic interactions, yielded bimetallic organometallic systems **3a,b**. The influence of the aurophillic interactions on the properties of the resulting chiral architectures carrying two Au(I)-alkynyl-helicene moieties has been examined in detail.

Results and Discussion

1. Monometallic Au(I) complexes 1a and (rac,P,M)-1b based on the 2,5-bis(2-pyridyl)phosphole ligand L1

The gold(I) precursor **4** (Scheme 1) was synthesized via the reaction of bis(2-pyridyl)phosphole **L1**[12a] with Au(tht)Cl according to a published procedure.[12b] Ethynyl-capped ligands **5a**, *rac*-**5b** and pure enantiomers *P*-(+)- and *M*-(-)-**5b** were prepared by previously described literature procedures.[11] Monometallic Au(I) precursor **4** was then reacted with either **5a** or (*rac*-, *P*-(+)- and *M*-(-)-) **5b** ligands to afford the complexes **1a** and *rac*-, *P*-(+)- and *M*-(-)-**1b**, respectively, in medium-to-good yields (Scheme 1). These phosphole-gold(I)-alkynyl-helicene complexes are stable in air and have good solubility in conventional polar solvents (e.g., CH_2Cl_2 and THF). They were characterized by multinuclear NMR spectroscopy, mass spectrometry, elemental analysis and single-crystal X-ray diffraction studies. The room temperature (r.t.) ^{31}P NMR spectra of complexes **1a** and **1b** in $CDCl_3$ show one singlet at 52.0 ppm and 51.9 ppm, respectively, i.e. the resonance is at higher frequency (downfield) compared to the singlet observed at 39.7 ppm for precursor **4**. The ^{1}H NMR spectra in $CDCl_3$ of these derivatives show the disappearance of the ethynyl proton of the free ligands **5a** and **5b** and reveal the expected 1:1 ratio for ethynyl/phosphole ligands (see the Supplementary Information, SI). Furthermore, the ^{13}C NMR spectra in $CDCl_3$ display two sharp singlets at 135.6 and 104.3 ppm (derivative **1a**) and at 135.5 and 103.3 ppm (*rac*-**1b**) for the respective C_α and C_β carbon atoms of the coordinated alkynyl fragments (see Table 1 for the C_α and C_β chemical shifts of all complexes). [13]



Scheme 1. Synthesis of complexes **1a** and *rac*-, *P*-, *M*-**1b** from phosphole-gold complex **4** and ethynyl-helicenes **5a**,**b** (60-76% yields).

Single crystals of derivatives **1a** and *rac*-**1b** were obtained at r.t. by diffusion of pentane into THF (**1a**) or CH_2Cl_2 (*rac*-**1b**) solutions (Table S3 in the SI). Both compounds yielded homogeneous batches of crystals and crystallize respectively in the *P*21/c and $P\bar{1}$ space groups. In the case of the derivative **1a** (Figure 2a), the Au-(C≡C) moieties are almost linear, with P-Au-C_α angles of 172.99° and 173.01°, and Au-C_α-C_β angles of 173.9° and 170.6° (Table 2).[&] These values, together with the $C_\alpha \equiv C_\beta$ bond distances of 1.212 Å and 1.193 Å, are indicative of gold(I)-alkynyl complexes.[14,15] As expected, the carbo[4]helicene fragment is not planar in the solid-state structure and displays a helicity degree of 30.7-31.6°, which is similar to what is reported in the literature.[11,16] All the other structural parameters related to the "Au-**L1**" fragment are classical.

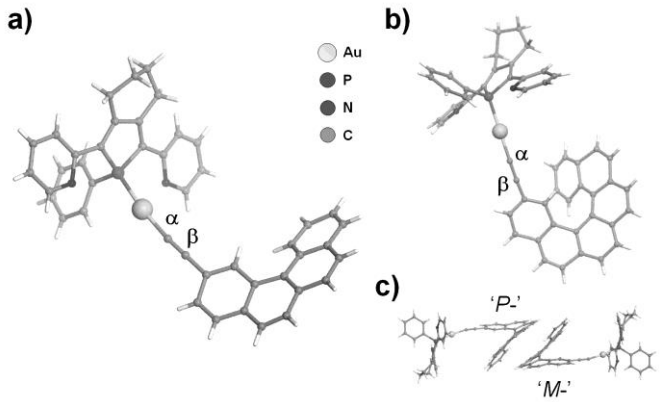


Figure 2. Views of the X-ray structures of (a) **1a** (only one of the two symmetrically independent molecules found in the unit cell of **1a** is shown); (b) *rac*-**1b** (only *M*-(+)-stereoisomer is shown) and (c) heterochiral π-dimers observed in the centrosymmetric crystal of *rac*-**1b**.

The solid-state examination of the complex *rac*-**1b** (Figure 2b) reveals the centrosymmetric unit cell with two enantiomers bearing either a *P*- or a *M*- carbo[6]helicene moiety. The expected molecular structure exhibits metric data being very similar to those of **1a** {P-Au-C_α angle, 173.04°; Au-C_α-C_β angle, 168.4°; $C_\alpha \equiv C_\beta$ bond distance, 1.211 Å (Table 2)}. The carbo[6]helicene fragment within **1b** has a helicity of 52.5° which is comparable with other [6]helicene ligands, showing that complexation to Au(I) occurs without generating any steric constraint.[11,16] Conversely to derivative **1a**, for which no specific intermolecular interactions were observed, the solid-state packing of *rac*-**1b** displays heterochiral π-stacked dimers (Figure 2c) resulting from weak intermolecular π-π interactions between neighboring molecules (ca. 3.7 Å). The photophysical properties (UV-vis and luminescence) of Au(I)-complexes **1a** and *rac*-**1b** were then investigated (Table S2 in the SI).[3e-h,10] The UV-vis absorption spectra were recorded in degassed dichloromethane at 298 K, while emission spectra were measured in both degassed dichloromethane at 298 K, and in EPA glass at 77 K (EPA = diethylether / isopentane / ethanol 2:2:1 v/v). The UV-vis absorption spectra of complexes **1a** and *rac*-**1b** (Figures S13 and S14) exhibit several intense bands between 250-360 nm with high absorption coefficients ($\varepsilon > 10^3$ M^{-1} cm^{-1}), and a broader band centered at 390 nm ($\varepsilon \sim 1.4 \times 10^3$ M^{-1} cm^{-1}). At 298 K, the luminescence spectra of complex **1a** and *rac*-**1b** correspond to the superimposition of fluorescence of the helicene moiety (centered at 409 nm and 440 nm for **1a** and *rac*-**1b**, respectively), and fluorescence of the phosphole π-system (centered at 475 and 470 nm for **1a** and *rac*-**1b**, respectively; see Figures S13 and S14, and Table S2). This superimposition of emissions from the two independent π-conjugated parts of the complexes results at 77 K in a mixture of fluorescence signals (**1a**, 470 nm; *rac*-**1b**, 440 nm) accompanied by structured phosphorescence bands observed at wavelengths above 520 nm for **1a** and above 530 nm for *rac*-**1b**. Such behaviour, with emission signals from essentially independent parts of the molecule, has already been observed in former helicene-phosphole derivatives.[16b] The 77 K phosphorescence bands are attributable to the helicene unit. The quantum yields of 298 K fluorescence assigned to helicene units are very low (**1a**, 0.4%; *rac*-**1b**, 0.3%) in comparison to ligands **5a**,**b** (7% and 3%, respectively) perhaps due to less rigid structures in **1a**,**b** leading to more efficient non-radiative emission pathways. Note that in complexes **1a**,**b**, there is probably no significant involvement of $^3[\sigma(\text{Au-P})\rightarrow\pi^*(\text{C}\equiv\text{C})]$ or metal-perturbed intraligand (IL) $^3[\pi\rightarrow\pi^*(\text{C}\equiv\text{C})]$ mixed with metal-to-alkynyl charge transfer (CT) excited states,[10] since the temporal decay of the phosphorescence signal occurs on a timescale of seconds (see Table S2) which is typical of helicenes. In contrast, a significant involvement of the heavy Au(I) centre (with its high spin-orbit coupling constant) in the excited state would be anticipated to promote intersystem crossing and lead to phosphorescence lifetimes of the order of microseconds. These observations and interpretations are supported by the calculations. Details are discussed below.

Table 1. The ^{13}C NMR chemical shifts of the C_α and C_β carbons in ppm ($CDCl_3$, r.t.)

	5a	**5b**	**1a**	**1b**	**2a**	**2b**	**3a**	**3b**
C_α	77.6	76.1	135.6	135.5	N.a.[a]	N.a.[a]	N.a.[a]	N.a.[a]
C_β	84.6	83.7	104.3	103.3	104.6	105.6	104.7	103.7

[a] Not assigned.

The chiroptical properties (optical rotation, OR, and electronic circular dichroism, ECD) of enantiopure *M*- and *P*-**1b** were studied next. Interestingly, the molar rotations (MRs) are almost doubled upon introducing the phosphole-gold(I) moiety, ($[\phi]_D^{23}$ in °cm^2/dmol: *P*-**5b**, +11030 (calc. BHLYP/SV(P) 17002);[11b,c,d] *P*-**1b**, +21340 (calc. 23575), Table S1). The difference in the chiroptical properties of **1b** and **5b** enantiomers is also reflected in their corresponding mirror-image ECD spectra. (Figure 3). As for most organic helicenes with *P*-stereochemistry[6] the ECD spectrum of *P*-**5b** displays a set of intense negative bands between 240-280 nm and a set of intense positive bands between 320-380 nm tailing down to 430 nm.[11b,c,d] A strong effect of the coordination of the [6]helicene-ethynyl fragment on the Au(I)-phosphole moiety is observed in the ECD spectra of *M*- and *P*-**1b** complexes, with an intensity enhancement below 300 nm as compared to *M*- and *P*-**5b**, and the appearance of a new band at 286 nm. Beyond 300 nm, the enhancement is also very important as the intensity of the ECD spectra of the *P* and *M* enantiomers of complex **1b** are almost twice those of the free ethynyl-capped carbo[6]helicene ligand **5b**. Such a strong modification of the ECD upon coordination was quite unexpected considering the weak interaction between closed-shell d^{10} gold(I) and the ethynyl-helicene ligands.

BHLYP/SV(P) TDKS calculations of the chiroptical properties , using BP/SV(P)-optimized molecular structures, were performed. Scalar relativistic effects were treated implicitly by the use of a 60-electron relativistic effective core potential (ECP) for Au. The *P*-**1b** excitations in the low-energy (long-wavelength) positive ECD band of the simulated electronic spectrum, with the strongest rotatory strengths, i.e. no. 3 (*E* = 359 nm), no. 4 (347), and no. 6 (323 nm, see Figure 4, Table S4 in the SI), involve

dominantly intraligand (IL) π-π* contributions in the helicene system. In terms of individual molecular orbital (MO) pairs the contributions are: HOMO - LUMO+1 (61%) for excitation no. 3, HOMO - LUMO+2 and HOMO-1 - LUMO+1 (37 and 28%) for no. 4, and HOMO-1 - LUMO+2 and HOMO-1 - LUMO+1 (38 and 17%) for no. 6. The reader is reminded that an excitation may have contributions from several occupied-unoccupied MO pairs, and that in TDKS the percentages may depend on the functional. These excitations are further assigned as having partial charge-transfer character since *i*) they involve orbitals centered in different parts of the π-system (compare HOMO with LUMO+1 and LUMO+2) and/or *ii*) they have non-negligible contributions from occupied and unoccupied MOs centered on different moieties (for example HOMO-1 - LUMO (12%) for no. 4 and HOMO-5 - LUMO (12%) for no. 6) which may be assigned as a classical ligand-to-ligand charge-transfer (LLCT) transitions from π(helicene) to π*(phosphole). Electronic conjugation between the two π-systems (i.e. helicene and phosphole) is not observed. One of the two π-orbitals constituting the triple bond C≡C is conjugated with the helicene π-system ($\pi_{||}$ = HOMO), while the other is perpendicular to the helicene π-system ($\pi_{\perp}$) and contributes to two MOs, HOMO-4 and HOMO-5, that are centered in the phosphole. These two MOs constitute a nearly degenerate +/- pair of linear combinations of $\pi_{\perp}$ with a phosphole orbital and therefore the interaction of $\pi_{\perp}$ with the phosphole is actually quite weak. Au 5*d* contributions are visible in the orbital isosurface plots, but very small as expected for closed-shell d^{10} metal centers (Figure 4). However, a unique feature of the *P*-**1b** spectrum as compared to *P*-**5b** is the presence of excitations with moderate positive rotatory strengths at low energy that involve orbitals in the phosphole moiety. For instance, the *P*-**1b** excitation no. 1 (calculated at 417 nm) corresponds to essentially pure π–π* ligand-to-ligand charge-transfer (LLCT) from the helicene to the phosphole system (HOMO-LUMO). Excitation no. 2 (calc. 386 nm) involves π–π* transitions localized in the phosphole moiety with a partial charge-transfer character due to C≡C $\pi_{\perp}$ and metal d orbital involvement (HOMO-4 - LUMO, HOMO-5 - LUMO).

Table 2. Selected bond lengths and angles in the X-ray structures of the complexes **1a**, *rac*-**1b** and **2a**.

	Au–P	Au-C_α	C_α-C_β	P-Au-C_α	Au-C_α-C_β
1a[a]	2.2718(16) 2.2820(15)	1.991(6) 1.999(6)	1.193(8) 1.212(8)	172.99(17) 173.01(18)	170.6(6) 173.9(5)
***rac*-1b**	2.2715(11)	2.001(3)	1.211(5)	173.04(9)	168.4(3)
2a[b]	2.2808(18)	2.022(7)	1.184(10)	172.4(2)	169.8(6)

[a] two sets of data for each of the symmetrically independent molecules found in the unit cell; [b] one set of data due to the symmetry in the structure.

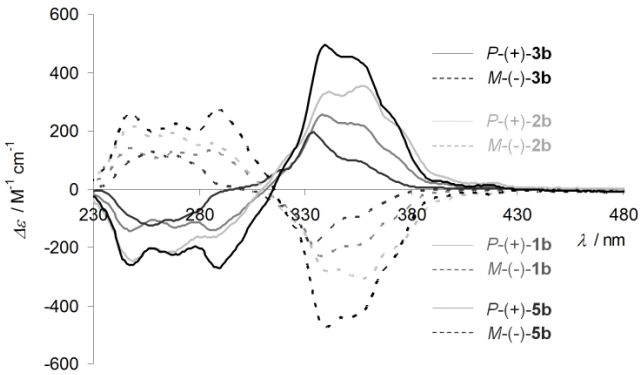


Figure 3. ECD spectra (~ 5 × 10^{-5} M in CH_2Cl_2) of the *P* and *M* enantiomers of ligand **5b** (red) and of phosphole-gold(I)-alkynyl-helicene complex **1b** (blue), bis-phosphole-bis[gold(I)-alkynyl-helicene] systems **2b** (green) and **3b** (black). Plain lines for *P* enantiomers and dotted lines for *M* enantiomers.

2. Dinuclear Au(I) complexes 2a and (*rac*-,*P*-,*M*-)-2b based on 2,2'-bisphosphole ligand L2

In a next step, the dinuclear gold(I) complex **6** stabilized by the 1,1',3,3',4,4'-hexamethyl-5,5'-bithienyl-2,2'-bisphosphole[9] ligand **L2** was used as a *U*-shape pre-assembled bimetallic molecular clip for the coordination-driven supramolecular organization of two ethynyl-capped carbo[4]- and carbo[6]helicene ligands, yielding **2a** and **2b**, respectively (Scheme 2). The 2,2'-bisphosphole **L2** displays an axial chirality generated by the bis-phosphole framework which is combined with the central chirality of the two phosphorus atoms and, together with the helical chirality of helicenes, the combinations of these three stereogenic elements can result in six possible stereoisomers (three pairs of enantiomers) in solution at r.t.[18] However, our group has previously shown that only two enantiomers of **6** (denoted [**6**]^{R}*RR* and [**6**]^{S}*SS*, see the SI) are observed in solution at r.t., as a result of diastereoselective coordination of the "Au(I)-iodide" fragments on the P-centers of **L2**, showing a single $^{31}P\{^{1}H\}$ NMR resonance at 37.7 ppm in CD_2Cl_2 for complex **6**.[9] The reason for such diastereoselective coordination is the aurophillic interaction (Au-Au = 3.050 Å) that takes place within **6** in a conformation that also minimizes the steric repulsion between the ring substituents. As a consequence, the metallophillic interaction 'locks' the 2,2'-bisphosphole subunit and the torsion angle between the mean planes of the two phosphole rings is fixed (ca. 48.0°).[9,18] Taking into account these structural and stereochemical features, dinuclear gold(I) precursor **6** was reacted with the π-conjugated ethynyl-capped ligands **5a** and *rac-, M-, P*-**5b** using the same synthetic procedure described for the mono-gold(I) complexes, thus yielding **2a** and *rac-*, (*M*,*M*)-, (*P*,*P*)-**2b**,[#] respectively, in good yields (80-84%; Scheme 2). These derivatives were obtained as air-stable solids of moderate solubility in conventional polar solvents (e.g. CH_2Cl_2, $CHCl_3$, THF). All these new compounds were fully characterized (see the SI).

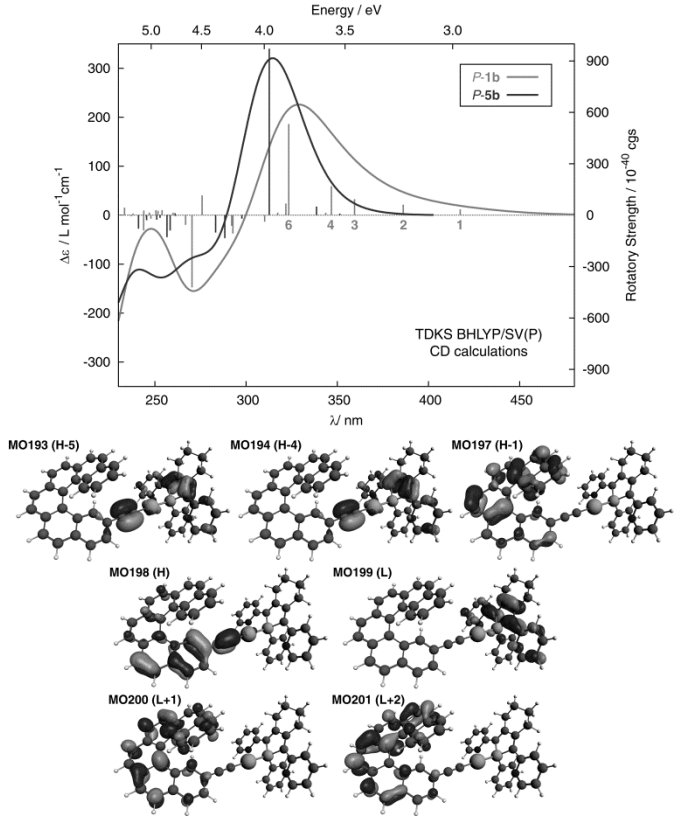
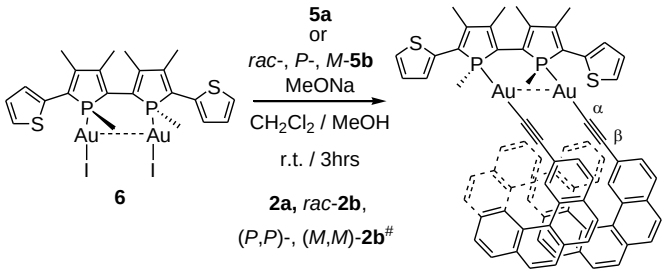


Figure 4. Top: comparison of the calculated ECD spectra of *P*-**5b** (red line)[11b,d] and *P*-**1b** (blue line). Numbered excitations correspond to those that were analyzed in detail (Table S4). No spectral shift has been applied. Bottom: isosurfaces (0.04 au) of MOs involved in selected transitions of the complex **1b**.



Scheme 2. Synthesis of the complexes **2a** and *rac*-, (*P*,*P*)-, (*M*,*M*)-**2b**[#] (80-84% yields).

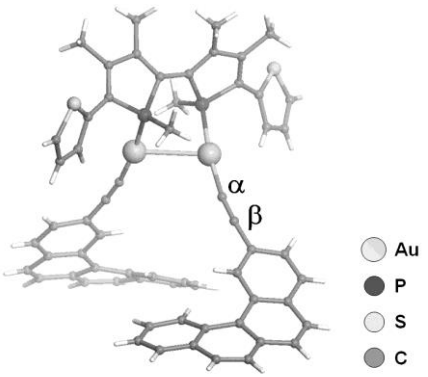


Figure 5. View of the X-ray structure of **2a** (only the [**2a**]^{S}*SS*(*PP*) enantiomer is shown).

The r.t. ^{31}P NMR spectrum of derivative **2a** in CD_2Cl_2 shows a singlet at 46.1 ppm, at higher frequency than **6** (37.7 ppm). Such a shift is similar to what was observed for **1a**,**b** and suggests the formation of one single complex in which two ethynyl-capped carbo[4]helicenes are coordinated to two Au(I) centers. The observation of only one singlet also suggests the formation of a racemic mixture in solution, similarly to what was observed in precursor **6**. In addition, the retention of the "Au_2(**L2**)" core bearing an aurophillic interaction and a blocked rotation of the two phosphole rings is maintained in the scaffold of **2a**. The complex **2a** displays a very simple symmetrical ^{1}H NMR spectrum at r.t. which shows the expected 1:2 biphosphole **L2**/ligand **5a** ratio. In the ^{13}C NMR spectrum, the C_β signal appears to higher frequency (104.6 ppm, Table 1) due to the coordination on the Au(I) centers, similarly to the derivatives **1a** and *rac*-**1b**. A homogeneous batch of single crystals was obtained by pentane vapor diffusion into a CH_2Cl_2 solution of **2a** which crystallized in the *C*2/c space group (Figure 5 and Table S3 in the SI).

The Au-(C ≡ C) moieties are almost linear with P-Au-C_α angle of 172.4° and Au-C_α-C_β angle of 169.8° (Table 2). The $C_\alpha \equiv C_\beta$ bond length is 1.184 Å. The twist angle between the mean plane of the two phosphole ring is ca. 42.7° which is smaller than the corresponding torsion angle in the dinuclear precursor **6** (ca. 48.0°).[9] This might be explained by the sterically less demanding alkynyl fragments as compared to the iodine ligands present in **6**. The intermetallic distance in **2a** (3.0904 Å) is comparable to the corresponding value in **6** (3.0500 Å) and relevant for aurophillic interaction.[2] This suggests that the Au(I)-Au(I) distance is controlled by the 2,2'-bisphosphole scaffold in these dinuclear complexes. As expected, the carbo[4]helicene fragment is not planar in the solid state and displays a classical value for helicity of 35°. Notably, in the solid-state structure of each derivative **2a**, the two carbo[4]helicene fragments are homochiral. The space group (*C*2/c) is non-chiral and a mixture of two enantiomers, [**2a**]^{R}*RR*(*MM*) and [**2a**]^{S}*SS*(*PP*) is observed. Note, however, that in solution at r.t., the [4]helicene units are planar in average and therefore only two [**2a**]^{R}*RR* / [**2a**]^{S}*SS* enantiomers can be noticed. Finally, the intramolecular distances observed between the two carbo[4]helicene fragments in the solid state are too large (> 7 Å) for any short-contact interaction (such as π-π or π-CH interactions) between these two fragments. No specific intramolecular interactions between the two carbo[4]helicene moieties and/or the 2,2'-bisphosphole ligand **L2** are neither observed. This indicates that there are no significant steric constraints or short intramolecular contacts resulting from the substitution of the iodine atoms by the two ethynyl-capped carbo[4]helicene

fragments. This was further confirmed by NOESY experiments in solution that did not reveal any correlation peaks. As for the crystal packing, no specific intermolecular interactions were noticed and the molecules **2a** are shown to be well isolated from each other in the solid state. The introduction of two carbo[4]helicene moieties onto the "Au_2(**L2**)" U-shaped core readily occurs without generating any specific steric constrains along the backbone of **2a**. These observations have triggered us to extend this reaction to the use of the larger ethynyl-capped carbo[6]helicene ligand *rac*-, *P*- and *M*-**5b**.

The reaction of two equivalents of ethynyl-capped carbo[6]helicene ligand *rac*-**5b** with the dinuclear Au(I) precursor **6** was first performed (Scheme 2) affording *rac*-**2b** complex (80% yield). Its r.t. ^{31}P NMR spectrum in CD_2Cl_2 shows four singlets between +45.3 and +45.8 ppm (Figure S9) shifted to higher frequency compared to **6**. These signals are assigned to the three different enantiomeric pairs of diastereoisomers (in a 1:1:2 ratio) present in solution resulting from the combination of the stereoisomers related to the "Au_2(**L2**)" scaffold (([**6**]^R*RR* and [**6**]^S*SS* enantiomers) with those related to the carbo[6]helicene moiety (*P* and *M* stereoisomers). The reaction therefore yields C_2-symmetrical [**2b**]^R*RR*(*MM*)/[**2b**]^S*SS*(*MM*) (and their mirror-images) and C_1-symmetrical [**2b**]^R*RR*(*MP*) (and its mirror-image) complexes, (see the SI for a detailed description of the diastereoisomeric mixture obtained and the assignment of the ^{31}P NMR spectrum signals). The r.t. ^{1}H NMR and ^{13}C NMR spectra of these derivatives are rather complicated, as a result of the superimposition of signals belonging to particular diastereoisomers.

Nevertheless, reacting precursor **6** with two equivalents of enantiopure ligands *M*- or *P*-**5b** afforded enantiopure (*M,M*)-**2b**$^{\#}$ or (*P,P*)-**2b**$^{\#}$ enantiomeric complexes, displaying two singlets in their r.t. ^{31}P NMR spectra in CD_2Cl_2 due to the different [**2b**]^R*RR* and [**2b**]^S*SS* stereochemistries around the axial and central phosphorus chiralities (see Figure S9). As a result, only two signals at +45.4 and +45.7 ppm corresponding to the [**2b**]^R*RR*(*MM*) and [**2b**]^S*SS*(*MM*) diastereoisomers (and their mirror-images) are observed. The r.t. ^{1}H NMR spectrum in $CDCl_3$ is well defined and clearly exhibits two sets of signals assigned to each diastereoisomer (see the SI). In other words, for each *M* or *P* helicene enantiomer, the 2,2'-bisphosphole moiety can adopt either the *R* or the *S* axial chirality, which in turn fixes the chirality of the P-atoms.

Unlike the phosphole-Au(I)-alkynyl-helicene **1a,b** complexes, the bis-phosphole-bis[Au(I)-alkynyl-helicene] complexes **2a**,**b** are not emissive. The UV-vis absorption spectra in CH_2Cl_2 of complex **2a** (Figure S15) exhibits strong bands at 240 and 295 nm with very high absorption coefficients ($\varepsilon \sim 1.1 \times 10^5$ M^{-1} cm^{-1}), several other bands between 310-380 nm ($\varepsilon > 1.6 \times 10^4$ M^{-1} cm^{-1}) and a broad one centered at 405 nm ($\varepsilon \sim 1.2 \times 10^3$ M^{-1} cm^{-1}), while *rac*-**2b** (Figure S16) displays two strong bands at 240 and 266 nm with very high absorption coefficients ($\varepsilon \sim 1.2 \times 10^5$ M^{-1} cm^{-1}), several other bands between 310-380 nm ($\varepsilon > 1.2 \times 10^5$ M^{-1} cm^{-1}) and a broad one centered at 425 nm ($\varepsilon \sim 1.7 \times 10^3$ M^{-1} cm^{-1}).

The optical activity of enantiopure (*P,P*)-**2b**$^{\#}$ and (*M,M*)-**2b**$^{\#}$ complexes was then investigated. First of all, a strong effect of the coordination of two alkynyl-helicenes onto bis-phosphole-bis-gold fragment was observed on the optical rotations since the MR of (*P,P*)-**2b** is three times bigger than that of ligand **5b** ($[\phi]_D^{23}$ in °cm^2/dmol: *P*-**5b**, +11030; (*P,P*)-**2b**, +35290). First-principles calculations were performed for **2b** in order to shed light on the structure-chiroptical properties relationships. Figure 6 displays the optimized molecular structures for selected, stable, low-energy conformers of **2b** in its [**2b**]^R*RR*(*PP*) and [**2b**]^S*SS*(*PP*) stereochemistry. For a given axial chirality of bis-Au(I)-bis-phosphole fragment a variety of nearly-degenerate conformers are obtained by rotation around the Au-C bonds. Based on KS energies obtained with the BP functional, the [**2b**]^R*RR*-based complexes are however in general more stable than [**2b**]^S*SS* systems. The calculated molar rotations depend strongly on the positions (distance and orientation) of the [6]helicene units with respect to each other, with higher rotations when the two [6]helicene units are further from each other. The aforementioned effect has already been theoretically analyzed by us for Cu^I-bis(aza[6]helicene-phosphole) systems studied[16b] and can be attributed to excitonic coupling between the chromophore moieties.[7c] Although the effect may be controlled to some degree by the Au-Au interaction via influencing the relative distance and orientation of the helicenes, the calculations indicate that the Au-Au distance in and of itself is not the deciding factor when it comes to the large variations in the MRs (*vide infra*, Figure 6). Overall, the Boltzmann-average value for the calculated MRs of the low-energy **2b** conformers presented in Figure 6 is 47766 °cm^2/dmol. The agreement is not quantitative. There may be additional conformers contributing to the MR, but the size of the molecules renders a complete conformational search as too demanding computationally. Another source of error is that many KS functionals have difficulties with the description of aurophillic interactions.[19] It has been noted previously[19] that non-hybrid local density approximation (LDA) functionals such as Xα can produce reasonably short Au-Au distances for small 'benchmark' systems containing Au(I). Indeed, we find that the average optimized Au-Au contacts for the three lowest-energy conformers increase from 3.0 to 3.3 to 3.5 Å, when going from Xα to BP to the hybrid functional B3LYP, with the shortest distance calculated with Xα being typical for aurophillic bonds. However, Xα produces poor structural parameters for the organic substituents, and the BHLYP MRs from these structures are in general unreliable (see Tables S12-S13 and Figure S32 in the SI). With the B3LYP structures, the Boltzmann-averaged MR is 34153 °cm^2/dmol and in very good agreement with experiment. The comparison of the MRs obtained with different sets of optimized structures shows that, for **2b**, the quality of the optimized Au-Au distance may therefore be less of a factor than the internal and relative geometries of the chromophores. Overall, the calculations are in agreement with experiment in that there is a strong enhancement of the MR when going from **5b** to **2b**.

The experimental ECD spectra of the (*M,M*)- and (*P,P*)-**2b** show a large intensity enhancement in the whole spectral region compared to the ECD of enantiopure ligand *M*- and *P*-**5b** (for instance, at 250 nm: *P*-**5b**: $\Delta\varepsilon$ = -105 M^{-1} cm^{-1}; (*P,P*)-**2b**: $\Delta\varepsilon$ = -243 M^{-1} cm^{-1}; at 356 nm: *P*-**5b**: $\Delta\varepsilon$ = +95 M^{-1} cm^{-1}; (*P,P*)-**2b**: $\Delta\varepsilon$ = +352 M^{-1} cm^{-1}) with new bands appearing at 290 nm and around 400 nm of medium and weak intensity, respectively (Figure 3). The effect is similar to that observed for mono-gold(I)-phosphole derivative **1b** but visibly stronger. The simulated Boltzmann-averaged ECD spectrum of the enantiopure (*P,P*)-**2b** qualitatively agrees well with experiment (Figure 7) enabling to understand

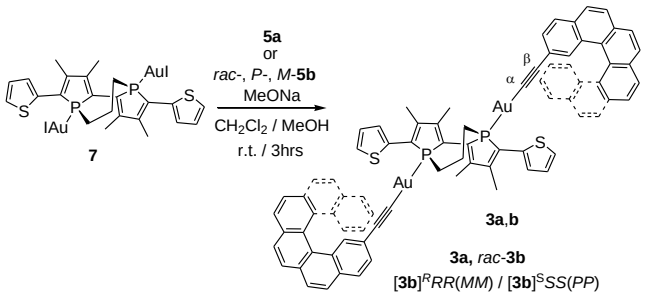
better relationships between molecular structure of **2b** and the resulting chiroptical properties.

Despite quite similar spectral envelopes calculated for different conformers of both [**2b**]^{R}*RR*(*PP*) and [**2b**]^{S}*SS*(*PP*) (see Figure S20 in the SI), two main differences can be noticed. (*i*) Structures with the *R* axial chirality afford higher intensity of the main positive ECD band around 350 nm. (*ii*) Conformers of [**2b**]^{S}*SS*(*PP*) generally demonstrate additional positive intensity in the low-energy part of the spectra (~ 430 nm) while for [**2b**]^{R}*RR*(*PP*) structures a negative band appears in this region. Both features go hand in hand with ECD spectra calculated for *R* and *S* enantiomers of the model system based on **2b** in which helicene moieties were replaced by phenyl groups (*vide infra*; for details see Tables S5-S7, S10 and Figures S21-24, S28-29).

Similarly to complex **1b**, an inspection of the molecular orbitals of **2b** shows no evidence of electronic conjugation between the helicene and phosphole π-systems through the gold center (see Figure 8 and the SI). A detailed analysis of dominant excitations in the low- and medium-energy parts of the simulated spectra of selected (*P,P*)-**2b** conformers indicates that the low-energy (long-wavelength) tail of the first ECD band is caused by excitation no. 1 calculated at 430 nm. The excitation can be assigned as an almost pure intraligand (IL) π-π* transition within the bis-phosphole system and, in line with the ECD spectra of the *R* and *S* stereoisomers of the model complex, it affords moderately intense negative / positive rotatory strength for [**2b**]^{R}*RR*(*PP*) / [**2b**]^{S}*SS*(*PP*). For example, excitation no. 1 in [**2b**]^{R}*RR*(*PP*)-2 and [**2b**]^{S}*SS*(*PP*)-1 corresponds to nearly pure HOMO-5 - LUMO transitions with rotatory strengths of -168 and 143 times 10^{-40} esu^2 cm^2, respectively, in cgs units. On average the ECD intensity therefore cancels out, as demonstrated by the simulated ECD spectrum of (*P,P*)-**2b** in Figure 7. Similar to the mono-Au(I) complex **1b**,the most intense (*P,P*)**-2b** excitations creating the main positive ECD band calculated between 330 and 315 nm, such as no. 11-13 ([**2b**]^{R}*RR*(*PP*)-1) and 12-14 ([**2b**]^{R}*RR*(*PP*)-2 and [**2b**]^{S}*SS*(*PP*)-1), reveal a mixed character of helicene IL π-π* (HOMO-2, HOMO-3, LUMO+4, LUMO+5) and ligand-to-ligand charge transfer (LLCT) involving helicene-centered MOs (HOMO-1, HOMO, Figure 8) and orbitals centered on the 2,2'-bisphosphole unit (LUMO, LUMO+1). Based on the results calculated for the model system, this type of LLCT transition may give opposite (positive / negative) ECD signature for *R* / *S* axial configuration in this energy region, which would account for the increase in the band intensity for [**2b**]^{R}*RR*(*PP*) as compared to [**2b**]^{S}*SS*(*PP*). The experimentally observed increase in the ECD intensity of the complex **2b** above 350 nm as compared to the pristine ligand **5b** and monometallic system **1b** originates mainly from intense excitations calculated between 400 and 340 nm that correspond to IL π-π* transitions localized in the helicene moieties mixed with contributions from IL π→π* within phosphole and / or LLCT from the helicenes to bis-phosphole fragment; for example no. 3, 4, 6, and 8, and no. 5, 6, 9 for [**2b**]^{R}*RR*(*PP*)-1, and [**2b**]^{R}*RR*(*PP*)-2, respectively, and no. 5, 8, 9 in the case of [**2b**]^{S}*SS*(*PP*)-1 (see the SI). All these transitions are stronger for (*P,P*)-**2b** due to reinforcing effects of two ethynyl-helicene ligands and the extended π-conjugated bis-phosphole unit which in consequence leads to an increase in the optical rotation of the bis-Au(I) system as compared to **1b**.

3. Dinuclear Au(I) complexes 3a and (*rac*-,*P*-,*M*-)-3b based on 2,2'-bisphosphole ligand L3

In a next step, the dinuclear gold(I) complex **7** (Scheme 3), obtained from bis-phosphole ligand **L3**, and whose conformation is consequently restricted due to the presence of the covalent (-CH_2-)$_3$ bridge, was used. We have previously shown that in this case, formation of the Au(I)-Au(I) interaction is prevented.[9] Therefore, the coordination of two ethynyl-capped carbo[4]helicene ligands **5a** yielded bimetallic complex **3a** (85% yield, see the SI) displaying no aurophillic interaction (Scheme 3). Its ^{31}P NMR spectrum in $CDCl_3$ at 45.6 ppm that is 14.8 ppm higher compared to **7**. The r.t. ^{1}H NMR of this derivative is simple, suggesting a symmetrical molecular structure bearing a 2:1 bis-phosphole **L3** / ligand **5a** ratio. The r.t. ^{13}C NMR spectrum shows a signal for carbons C_β (104.7 ppm, Table 1).



Scheme 3. Synthesis of the complexes **3a** and *rac*-, (*P,P*)-, (*M,M*)-**3b**$^{\#}$ (80-85% yields).

The racemic derivative **3b** was then synthesized via the reaction of two equivalents of racemic ligand **5b** with complex **7** (82% yield) and was fully characterized. Its r.t. ^{31}P NMR spectrum in CD_2Cl_2 shows a singlet at 46.1 ppm. At 183 K, the ^{31}P NMR spectrum shows four signals, similarly to what was observed for the racemic derivative **2b** (vide supra). These signals arise from the three different diastereoisomers present in solution [**3b**]^{R}*RR*(*MM*), [**3b**]^{S}*SS*(*MM*), [**3b**]^{R}*RR*(*MP*) (1:1:2 ratio) and their related mirror images (see Figure S11 in the SI). The fact that the diastereoisomers are distinguished at low temperature but not at r.t. probably arises from restricted conformations upon cooling.

Note that the same situation is observed for the enantiopure complex **2b** for which, upon increasing the temperature, the two signals observed in the ^{31}P NMR spectrum merge into one signal (Figure S10). The r.t. ^{1}H NMR spectrum in CD_2Cl_2 reveals the presence of one set of signals and is simple, suggesting a molecular structure having a 2:1 biphosphole **L3** / ligand **5b** ratio. The r.t. ^{13}C NMR spectrum shows a signal for carbons C_β at 103.7 (Table 1). The enantiopure (*M,M*)- and (*P,P*)-**3b**$^{\#}$ were then prepared from *M*- and *P*-**5b** using the same procedure (80% yield). Here again, the formed diastereoisomers could not be distinguished on the NMR timescale, except at low temperatures (183 K), at which the two formed diastereoisomers [**3b**]^{R}*RR*(*MM*), [**3b**]^{S}*SS*(*MM*) (or their mirror-images) show two distinct signals at 43.7 and 43.6 ppm in the ^{31}P NMR spectra (Figure S12). The UV-vis spectrum of **3a** / **3b** is very similar to the one of **2a** / **2b**, but with slightly stronger / weaker absorption in the 430-480 nm region (see Figure S15 and S16).

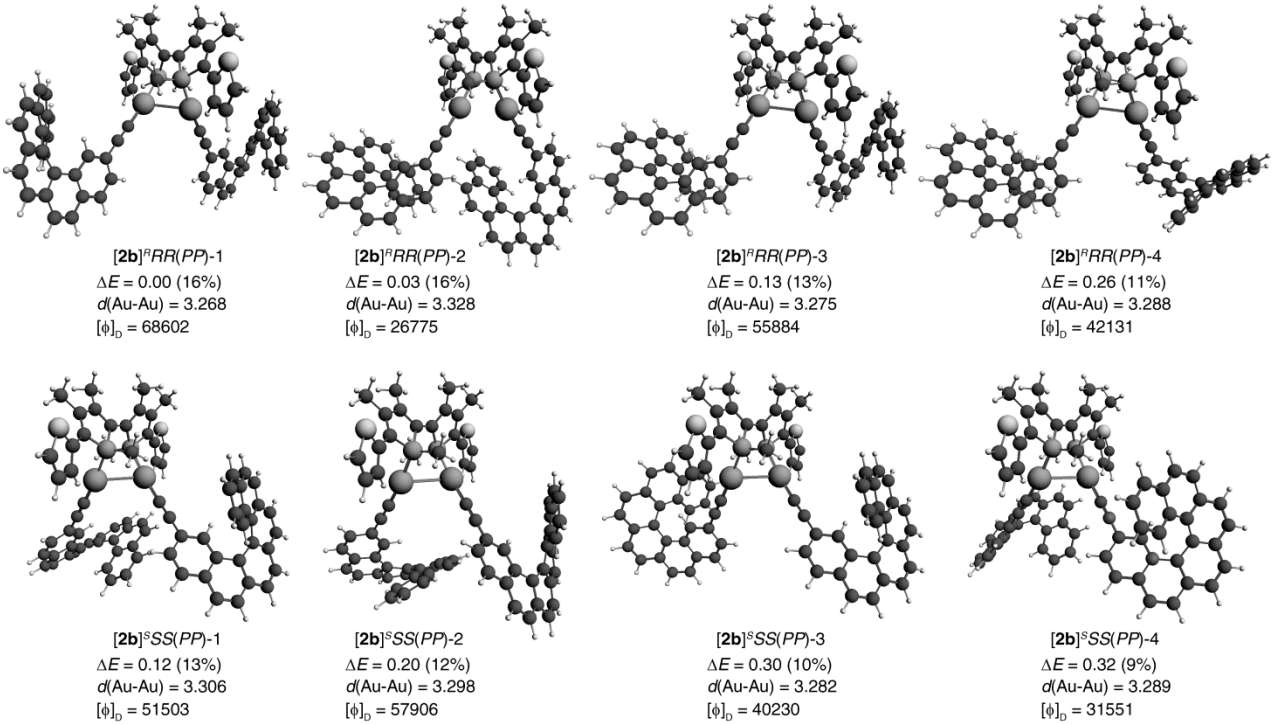


Figure 6. BP/SV(P)-optimized molecular structures of selected low-energy conformers of complex **2b**. The *P* helicity is used for helicenes, and both *R* and *S* axial chirality is examined. Values listed correspond to relative energies, ΔE in kcal/mol (in parentheses the corresponding Boltzmann populations are given in %), Au–Au distances, *d*(Au–Au) in Å, and molar rotations, $[\phi]_D$ in °cm^2/dmol.

A comparison between the molar rotations measured for enantiopure (*P,P*)-**3b** derivatives and for ligand **5b** reveals again a strong effect of the coordination of two ethynyl-[6]helicene moieties on the bis-phosphole bis-gold scaffold ($[\phi]_D^{23}$ in °cm^2/dmol: *P*-**5b**, +11030; (*P,P*)-**3b**, +43400) despite the presence of two [**3b**]^R*RR*(*PP*), [**3b**]^S*SS*(*PP*) diastereoisomers originating from the two possible *R* and *S* axial chirality. Here again, the axial chirality appears to have no substantial influence on the chiroptical properties (compare with Figure 9 and the SI). Very interestingly, the MR is even higher than those of the derivative **2b**, and highlights the influence of the aurophillic interaction. Indeed, in the case of (*P*,*P*)-**3b**, for which no aurophillic interaction can take place, the two helicene units are separated from each other, while in the complex **2b** they may be put into close proximity due to the Au(I)-Au(I) interaction. Furthermore, although experimental ECD spectra of the (*M,M*) and (*P,P*) enantiomers of the complexes **2b** and **3b** show very similar bands, higher intensities are found for the derivative **3b** ((*P*,*P*)-**3b** $\Delta\varepsilon$ = +437 M^{-1} cm^{-1}, (*P*,*P*)-**2b** $\Delta\varepsilon$ = +352 M^{-1} cm^{-1} at 356 nm; Figure 3).

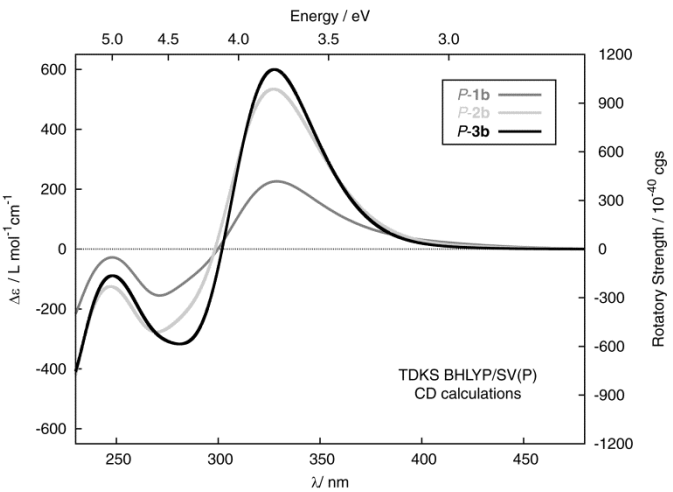


Figure 7. Comparison of the calculated ECD spectra of *P*-**1b** (blue line) and Boltzmann-averaged spectra for (*P*,*P*)-**2b** (green line) and for (*P*,*P*)-**3b** (black line) conformers. No spectral shift has been applied. See the SI.

The calculated (*P*,*P*)-**3b** MR of 44621 °cm^2/dmol and the corresponding ECD spectrum in Figure 7 agree well with experiment and therefore confirm that the chiroptical properties are directly related to the molecular structure. Again, the simulated spectrum and MR represent Boltzmann averages over several optimized low-energy conformers (Figure 9) that are

related to each other by rotation of the helicenes about the C-Au-P axes. The interactions are weak, leading to very small differences in energy, unlike for the aurophilic **2b** system. As a consequence, the helicene substituents of **3b** can undergo nearly free rotations. When the MR is calculated for 6 x 6 structures obtained from 60-degree rotations of the two helicenes about the C-Au-P axes starting from the lowest-energy ^{R}RR and ^{S}SS conformers, without further optimization, the average is 42051 °cm^2/dmol, which is again in very good agreement with experiment. As for the system **2b**, the low-energy tail of the first ECD band of **3b** originates from excitation no. 1 calculated around 400 nm for the different conformers (see Tables S8-9 and Figures S26-27). It is predominantly assigned as an IL π-π* transition within the bis-phosphole fragment. Again, on average the ECD intensities cancel due to typically opposite signs (positive / negative) for conformers with *R* / *S* axial chirality (see also results for the model complex based on **3b**, Figure S30-31 and Table S11 in the SI). The excitations calculated between 340 and 360 nm correspond mainly to IL π-π* transitions localized in the helicene moieties and although they partially cancel each other due to rotatory strengths of opposite signs they are in general more intense than in **2b**. The remaining intense excitations of the simulated spectra of selected (*P,P*)-**3b** conformers (ca. 330-320 nm) reveal similar assignment to (*P,P*)-**2b**, i.e. IL-helicene π-π* transitions and helicene→bis-phosphole LLCT. However, unlike for **2b**, they have on average more pronounced LLCT character which may rationalize their increased intensity as compared to **2b**. Overall, these results show that the farer the helicenes are positioned one to each other within the chiral architecture, the higher the chiroptical properties of the overall scaffold.

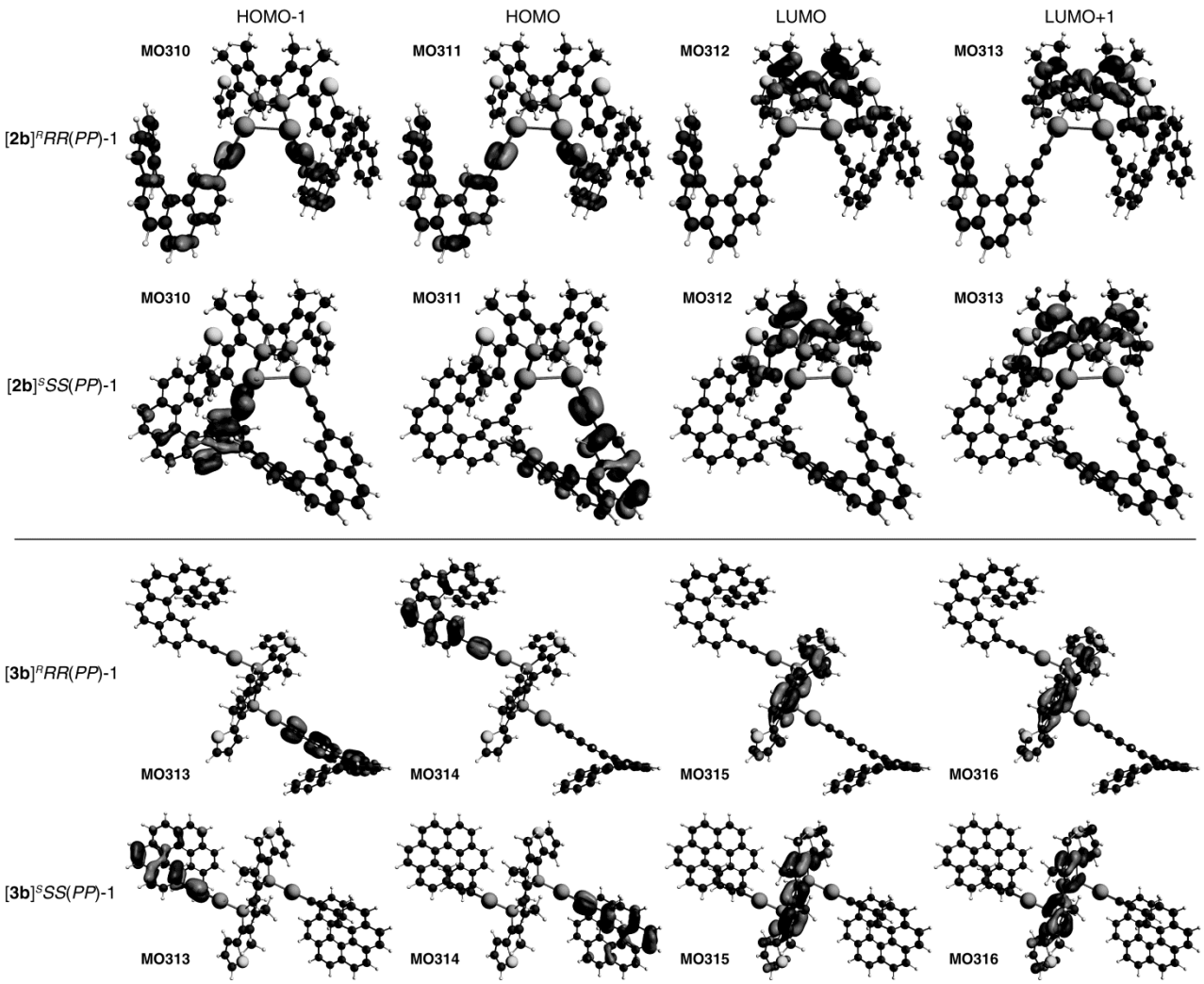


Figure 8. Isosurfaces (0.04 au) of frontier MOs of selected low-energy conformers of the complexes (*P*,*P*)-**2b** and (*P*,*P*)-**3b**.

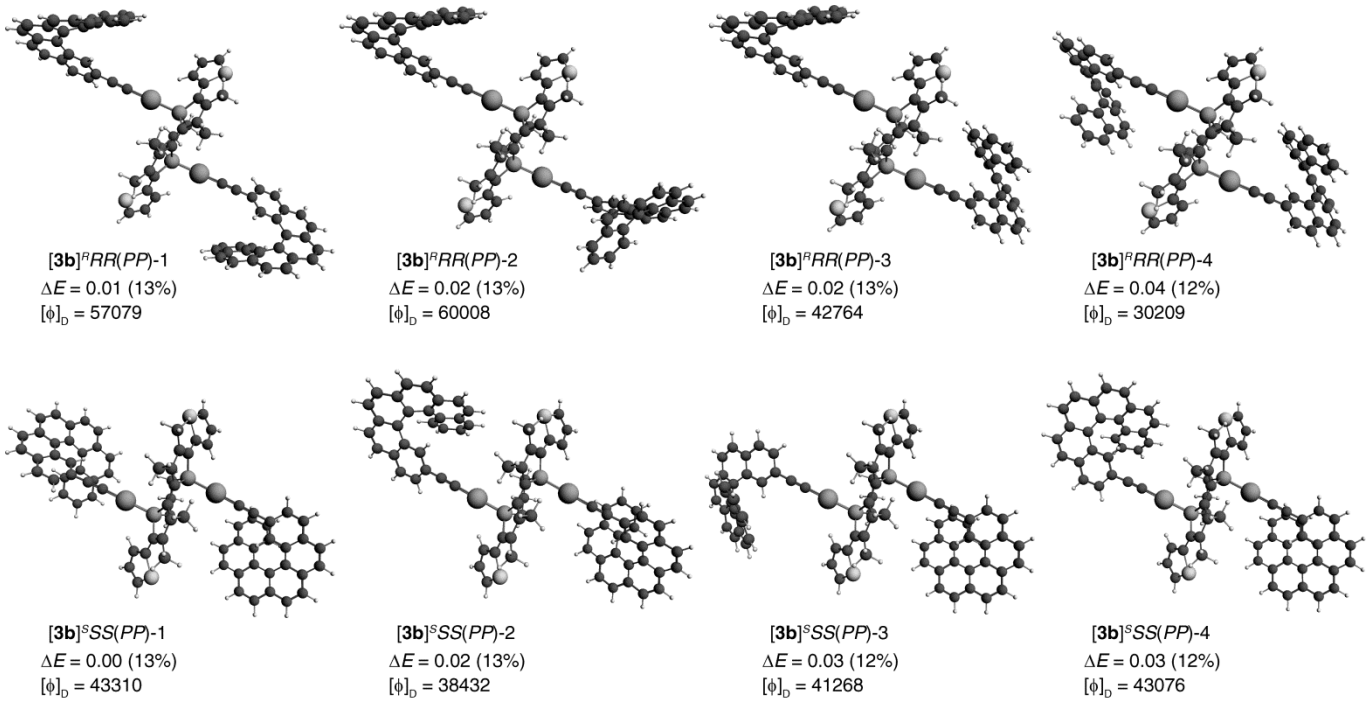


Figure 9. BP/SV(P)-optimized molecular structures of selected low-energy conformers of the derivative **3b**. The *P* helicity is used for helicenes, and both *R* and *S* axial chirality is examined. Values listed correspond to relative energies, ΔE in kcal/mol (in parentheses the corresponding Boltzmann populations are given in %), and molar rotations, in $[\phi]_D$ °cm^2/dmol.

Conclusions

We have demonstrated that molecular engineering of helicenes using simple gold(I) chemistry and phosphole π-conjugated ligand is a great tool to tune the chiroptical properties of helicene derivatives. Firstly, we have shown that a mono-phosphole gold(I) ('Au-**L1'**) complex displays significant enhancement of the chiroptical properties as compared to those of the corresponding parent helicene ligand, simply due to LLCT-type transitions from the helicene to the phosphole ligand. Secondly, we have used bimetallic molecular clips for the coordination-driven supramolecular organisation of two ethynyl-capped carbo[4]- and carbo[6]helicene ligands. The role of the gold-gold interaction in the generation of bis-helicene architectures with defined topologies has been highlighted with the use of either 'Au_2(**L2**)' U-shape or 'Au_2(**L3**)' Z-shape core, enabling or preventing aurophillic interactions, respectively. Its impact on the chiroptical properties has been demonstrated, with the disappearance of emission along with the increase of ECD intensities and molar rotation values as compared to mono-helicene mono-phosphole gold(I) complex. In the bis-helicene bis-phosphole bis-gold(I) architectures, the charge transfers from the helicene ligands to the bis-phosphole unit, together with the spatial proximity of the helicene ligands, have been shown to be the key features that influence these properties.

Acknowledgements

We thank the Ministère de l'Education Nationale, de la Recherche et de la Technologie, the Centre National de la Recherche Scientifique (CNRS) and the ANR (12-BS07-0004-METALHEL-01), the International Laboratories Rennes-Zhengzhou (IAL MOF), Rennes-Durham (IAL MMC), the National Natural Science Foundation (21272218), Specialized Research Fund for the Doctoral Program of Higher Education (20134101110004), Henan Science and Technology Department (no. 144300510011) and Zhengzhou Science and Technology Department (131PYSGZ204) of China, for their financial support. The theoretical component of this work has been supported by the National Science Foundation (CHE 1265833 to J.A.) and the Ministry of Science and Higher Education in Poland ('Outstanding Young Scientist' scholarship to M. S.-H.). M. S.-H. and J. A. acknowledge the Centre for Computational Research (CCR) at the University at Buffalo for providing computational resources.

Keywords: aurophillic interaction • helicene • phosphole • circular dichroism • chiral organometallic architecture

Notes

[&] The two sets of values are for each of the two symmetrically independent complexes found in the unit cell of the X-ray structure of **1a**.

[#] (*P*,*P*)-**2b**/**3b** refers to [**2b**/**3b**]^{R}*RR*(*PP*) and [**2b**/**3b**]^{S}*SS*(*PP*) while (*M*,*M*)-**2b**/**3b** refers to [**2b**/**3b**]^{R}*RR*(*MM*) and [**2b**/**3b**]^{S}*SS*(*MM*).

References

[1] See S. Sculfort, P. Braunstein, *Chem. Soc. Rev.* **2011**, *40*, 2741-2760 and references therein.

[2] a) P. Pyykkö, *Angew. Chem. Int. Ed.* **2004**, *43*, 4412-4456; b) P. Pyykkö, *Chem. Rev.* **1997**, *97*, 597-636; c) D. J. Gorin, F. D. Toste, *Nature* **2007**, *446*, 395-403.

[3] a) A. Laguna, *Modern Supramolecular Gold Chemistry*, Wiley-VCH, Weinheim, **2008**; b) R. J. Puddephatt, *Chem. Soc. Rev.* **2008**, *37*, 2012-2027; c) H. Schmidbaur, A. Schier, *Chem. Soc. Rev.* **2008**, *37*, 1931-1951; d) V. W. W. Yam, E.C.C. Cheng, *Chem. Soc. Rev.* **2008**, *37*, 1806-1813; e) V. W. W. Yam, K. M. -C. Wong, *Chem. Comm.* **2011**, *47*, 11579-11592; f) A. Johnson, A. Laguna, M. Concepcion Gimeno, *J. Am. Chem. Soc.* **2014**, *136*, 12812-12815; g) J. M. Lopez de Luzuriaga, in *Modern Supramolecular Gold Chemistry: Gold-Metal Interactions and Applications* (Ed. A. Laguna), Wiley-VCH, **2008**; pp 347−401; h) J. Lima, L. Rodríguez, *Chem. Soc. Rev.* **2011**, *40*, 5442-5456; i) N. Kobayashi, Y. Kamei, Y. Shichibu, K. Konishi, *J. Am. Chem. Soc.* **2013**, *135*, 16078-16081; j) V. W.-W. Yam, V. K.-M. Au, S. Y.-L. Leung, *Chem. Rev.* **2015**, *115*, 7589-7728.

[4] a) C. P. McArdle, S. Van, M.C. Jenning, R. J. Puddephatt, *J. Am. Chem. Soc.* **2002**, *124*, 3959-3965; b) S. Y. Yu, Z. X. Zhang, E.C.C. Cheng, Y.Z. Li, V.W.W. Yam, *J. Am. Chem. Soc.* **2005**, *127*, 17994-17995; c) V. Camara, N. Masciocchi, J. Gil-Rubio, J. Vicente, *Chem. Eur. J.* **2014**, *20*, 1389-1402.

[5] Selected reviews: a) X. -D. Zheng, T. -B. Lu, *CrystEngComm* **2010**, *12*, 324-336; b) F. Vera, J. L. Serrano, T. Sierra, *Chem. Soc. Rev.* **2009**, *38*, 781-796; c) W.; Lin, *J. Solid State Chem.* **2005**, *178*, 2486-2490; d) G. Seeber, B. E. F. Tiedemann, K. Raymond, *Top. Curr. Chem.* **2006**, *265*, 147-183; e) M. Yoon, R. Srirambalaji, K. Kim, *Chem. Rev.* **2012**, *112*, 1196-1231; f) J. Crassous, *Chem. Soc. Rev.* **2009**, *38*, 830-845; g) J. Crassous, *Chem. Comm.* **2012**, *48*, 9684-9692; h) G. A. Hembury, V. V. Borovkov, Y. Inoue, *Chem. Rev.* **2008**, *108*, 1-73.

[6] a) R. H. Martin, *Angew. Chem. Int. Ed.* **1974**, *13*, 649-660; b) T. J. Katz, *Angew. Chem. Int. Ed.* **2000**, *39*, 1921-1923; c) A. Urbano, *Angew. Chem. Int. Ed*. **2003**, *42*, 3986-3989; d) A. Rajca, M. Miyasaka, in *Functional Organic Materials* (Eds.: T. J. J. Müller, U. H. F. Bunz), Wiley-VCH, Weinheim, **2007**, pp. 543-577; e) F. Dumitrascu, D. G. Dumitrescu, I. Aron, *Arkivoc* **2010**, 1-32; f) Y. Shen, C. -F. Chen, *Chem. Rev.* **2012**, *112*, 1463-1535; g) M. Gingras, *Chem. Soc. Rev.* **2013**, *42*, 1051-1095; h) J. Bosson, J. Gouin, J. Lacour, *Chem. Soc. Rev.* **2014**, *43*, 2824-2840; i) N. Saleh, C. Shen, J. Crassous, *Chem. Sci.* **2014**, *5*, 3680-3694.

[7] a) D. Amabilino, *Chirality at the Nanoscale, Nanoparticles, Surfaces, Materials and more*, Wiley-VCH, **2009**; b) B. L. Feringa, W.R. Browne, *Molecular Switches*, Wiley-VCH, 2nd edition, **2011**; c) L. A. Nafie, in Comprehensive Chiroptical Spectroscopy (Ed.: N. Berova, P. L. Polavarapu, K. Nakanishi, R. W. Woody), Wiley-VCH: New York, **2012**, Vol. 2.

[8] a) F. Mathey,Phosphorus-Carbon Heterocyclic Chemistry: The rise of a new domai, Pergamon, Oxford, UK, **2001**; b) M. Hissler, P. Dyer, R. Réau, *Coord. Chem. Rev.* **2003**, *244*, 1-44; c) R. Réau, T. Baumgartner, *Chem. Rev.* **2006**, *106*, 4681-4727.

[9] H. Chen, W. Delaunay, L. Yu, D. Joly, Z. Wang, J. Li, Z. Wang, C. Lescop, D. Tondelier, B. Geffroy, Z. Duan, M. Hissler, F. Mathey, R. Réau, *Angew. Chem. Int. Ed.* **2012**, *51*, 214-217.

[10] a) K.-L. Cheung, S.-K. Yip, V. W.-W. Yam, *J. Organomet. Chem.* **2004**, *689*, 4451-4462; b) V. W.-W. Yam, K. M.-C. Wong, *Top. Curr. Chem.* **2005**, *257*, 1-32; c) M. J. Irwin, J.J. Vittal, R. J. Puddephatt, *Organometallics* **1997**, *16*, 3541-3547.

[11] a) M. El Sayed Moussa, K. Guillois, W. Shen, R. Réau, J. Crassous, C. Lescop, *Chem. Eur. J.* **2014**, *20*, 14853-14867; b) E. Anger, M. Srebro, N. Vanthuyne, L. Toupet, S. Rigaut, C. Roussel, J. Autschbach, J. Crassous, R. Réau, *J. Am. Chem. Soc.* **2012**, *134*, 15628-15631; c) M. El Sayed Moussa, M. Srebro, E. Anger, N. Vanthuyne, C. Roussel, C. Lescop, J. Autschbach, J. Crassous, *Chirality* **2013**, *25*, 455-465; d) M. Srebro, E. Anger, B. Moore, II, N. Vanthuyne, C. Roussel, R. Réau, J. Autschbach, J. Crassous, *Chem. Eur. J.* **2015**, *21*, 17100-17115.

[12] a) C. Hay, M. Hissler, C. Fischmeister, J. Rault-Berthelot, L. Toupet, L. Nyulaszi, R. Reau, *Chem. Eur. J.* **2001**, *7*, 4222-4236; b) M. Deponte, S. Urig, L. D. Arscott, K. Fritz-Wolf, R. Réau, C. Herold-Mende, S. Koncarevic, M. Meyer, E. Davioud-Charvet, D. P. Ballou, C. H., Williams, Jr., K. Becker, *J. Biol. Chem.* **2005**, *280*, 20628-20637.

[13] a) J. Vicente, M.-T. Chicolte, M.-D. abrisqueta, *J. Chem. Soc. Dalton Trans.* **1995**, 497-498; b) W. Lu, N. Zhu, C.-M. Che, *J. Organomet. Chem.* **2003**, *670*, 11-16.

[14] Selected examples of chiral gold-alkynyl complexes bearing P-ligands: a) I. R. Whittall, M. G. Humphrey, M. Samoc, B. Luther-Davies, D. C.R. Hockless, *J. Organomet. Chem.* **1997**, *544*, 189-196; b) T. J. Burchell, M. C. Jennings, R. J. Puddephatt, *Inorg. Chim. Acta* **2006**, *359*, 2812-2818; c) M. Weishaeupl, C. Robl, W. Weigand, S. Kowalski, F. Mohr, Fabian, *Inorg. Chim. Acta* **2011**, *374*, 171-174. For gold-complexes bearing phopshorated helicenes as ligands see: a) S. Cauteruccio, A. Loos, A. Bossi, M. C. Blanco Jaimes, D. R. Dova, F. S. Prager, A. Dreuw, E. Licandro, A. S. K. Hashmi, *Inorg. Chem.* **2013**, *52*, 7995-8004; b) K. Yavari, P. Aillard, Y. Zhang, F. Nuter, P. Retailleau, A. Voituriez, A. Marinetti, *Angew. Chem. Int. Ed.* **2014**, *53*, 861-865; c) K. Yavari, P. Retailleau, A. Voituriez, A. Marinetti, *Chem. Eur. J.* **2013**, *19*, 9939-9947.

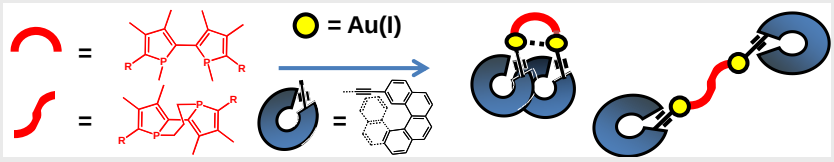
[15] Selected examples: a) V. W.-W. Yam, S. W. K. Choi, *J. Chem. Soc., Dalton Trans.* **1996**, 4227-4232; b) D. Li, X. Hong, C. M. Che, W. C. Lo, S. M. Peng, *J. Chem. Soc., Dalton Trans.* **1993**, 2929-2932; c) H. Y. Chao, W. Lu, Y. Li, M. C. W. Chan, C. M. Che, K. K. Cheung, N. Zhu, *J. Am. Chem. Soc.* **2002**, *124*, 14696-14706; d) W. Lu, N. Zhu, C.-M. Che, *J. Am. Chem. Soc.* **2003**, *125*, 16081-16088; e) M. Shiotsuka, N. Nishiko, Y. Tsuji, N. Kitamura, S. Onaka, K. Sako, *Transition Met. Chem.* **2010**, *35*, 129-135.

[16] a) E. Anger, M. Rudolph, L. Norel, S. Zrig, C. Shen, N. Vanthuyne, L. Toupet, J. A. G. Williams, C. Roussel, J. Autschbach, J. Crassous, R. Réau, *Chem. Eur. J.* **2011**, *17*, 14178-14198; b) S. Graule, M. Rudolph, W. Shen, C. Lescop, J. A. G. Williams, J. Autschbach, J. Crassous, R. Réau, *Chem. Eur. J.* **2010**, *16*, 5976-6005.

[17] V. Vreshch, M. El Sayed Moussa, B. Nohra, M. Srebro, N. Vanthuyne, C. Roussel, J. Autschbach, J. Crassous, C. Lescop, R. Réau, *Angew. Chem. Int. Ed.* **2013**, *52*, 1968-1972.

[18] a) M. Gouygou, O. Tissot, J.-C. Daran, G. G. A. Balavoine, *Organometallics* **1997**, *16*, 1008-1015; b) O. Tissot, M. Gouygou, F. Dallemer, J. -C. Daran, G. G. A. Balavoine, *Angew. Chem. Int. Ed.* **2001**, *40*, 1076-1078; c) E. Robe, W. Perlikowska, C. Lemoine, L. Diab, S. Vincendeau, M. Mikolajczyk, J. -C. Daran, M. Gouygou, *Dalton Trans*. **2008**, 2894-2898; d) E. Robé, C. Ortega, M. Mikina, M. Mikolajczyk, J.-C. Daran, M. Gouygou, *Organometallics* **2005**, *24*, 5549-5559.

[19] a) C. M. Aikens, *Molecular Simulation* **2012**, *38*, 607-614; b) S. -G. Wang, W. H. E. Schwarz, *J. Am. Chem. Soc.* **2004**, *126*, 1266-1276; c) F. Mendizabal, S. Miranda-Rojas, L. Barrientos-Poblete, *Comput. Theor. Chem.* **2015**, *1057*, 74-79; d) J. Muniz, E. Sansores, J. A. Reyes-Nava, V.-H. Ramos-Sanchez, A. Olea, *Int. J. Quantum Chem*. **2011**, *111*, 4378-4388.



Monometallic and bimetallic gold(I)-alkynyl-helicene complexes featuring the presence or absence of aurophillic intramolecular interactions have been prepared by using different types of phosphole ligands (mono-phosphole or bis-phospholes). The influence of the Au(I) d^{10}-metal center(s) on the electronic, photophysical and chiroptical properties has been examined.

Mehdi El Sayed Moussa [a] *Hui Chen,*[b,c] *Zuoyong Wang,*[b] *Monika Srebro-Hooper,*[d] *Nicolas Vanthuyne,*[e] *Soizic Chevance,*[a] *Christian Roussel,*[e] *J. A. Gareth Williams,*[f] *Jochen Autschbach* *,[g] *Régis Réau,*[a] *Zheng Duan,*[*,b] *Christophe Lescop,*[*,a] *and Jeanne Crassous*[*,a]

.

Bimetallic gold(I) complexes with ethynyl-helicene and bis-phosphole ligands: understanding the role of aurophillic interaction in their chiroptical properties